nature biotechnology

Article

https://doi.org/10.1038/s41587-022-01636-0

Chem-map profiles drug binding to chromatin in cells

Received: 17 August 2022

Accepted: 6 December 2022

Published online: 23 January 2023

Check for updates

Zutao Yu[1,4], Jochen Spiegel[1,4], Larry Melidis[2], Winnie W. I. Hui[2], Xiaoyun Zhang[1], Antanas Radzevičius[1] & Shankar Balasubramanian[1,2,3]

Characterizing drug–target engagement is essential to understand how small molecules influence cellular functions. Here we present Chem-map for in situ mapping of small molecules that interact with DNA or chromatin-associated proteins, utilizing small-molecule-directed transposase Tn5 tagmentation. We demonstrate Chem-map for three distinct drug-binding modalities as follows: molecules that target a chromatin protein, a DNA secondary structure or that intercalate in DNA. We map the BET bromodomain protein-binding inhibitor JQ1 and provide interaction maps for DNA G-quadruplex structure-binding molecules PDS and PhenDC3. Moreover, we determine the binding sites of the widely used anticancer drug doxorubicin in human leukemia cells; using the Chem-map of doxorubicin in cells exposed to the histone deacetylase inhibitor tucidinostat reveals the potential clinical advantages of this combination therapy. In situ mapping with Chem-map of small-molecule interactions with DNA and chromatin proteins provides insights that will enhance understanding of genome and chromatin function and therapeutic interventions.

Small molecules that interact with cellular DNA formed the basis for early anticancer molecules that became widely deployed in the clinic[1]. A greater understanding of genome structure and function has created new opportunities for intervening with biology and disease states by targeting cellular DNA or the associated proteins with small molecules. It is essential to validate target engagement for molecular probes and therapeutic drugs. Mapping where a small molecule binds chromatin can help explain the downstream genetic or epigenetic response[2]. However, mapping inhibitors to chromatin-associated proteins has proved challenging and is limited to a few high-affinity ligands, including the bromodomain inhibitor JQ1 and the CDK9 inhibitor AT7519 using Chem-seq or related approaches[3–6]. Existing methods involve the binding of small molecules to sheared chromatin followed by enrichment using an affinity tag. Such approaches require high ligand binding affinity and low dissociating rates and suffer from weak signal and high background, together with potential epitope masking upon excessive formaldehyde cross-linking. Furthermore, the requirement for large amounts of input material (typically tens of millions of cells) precludes applications involving low cell numbers or rare epitopes[3]. The detection of binding sites for small molecules that bind directly to cellular DNA has proved to be largely elusive. Some binding sites have been inferred by mapping downstream DNA damage response or break events[7–11]. While direct detection has been achieved for DNA minor groove binding molecules to synthetic DNA oligonucleotides[12,13] and for the intercalator psoralen UV-crosslinked to DNA in cells[3,14], a practical challenge for noncovalent small-molecule–DNA interactions is dissociation during washing steps and sample processing[4]. Therefore, many approved, widely used drugs thought to act via a DNA targeting modality have, remarkably, not yet had their cellular molecular targets validated. In situ maps of small-molecule–DNA interactions in intact cells would provide valuable insights into the mode of action of this family of drugs and enhance our ability to exploit the genome as a therapeutic target.

Herein we report a general approach, Chem-map, to establish in situ interaction maps for small molecules that bind to cellular genomic

[1]Yusuf Hamied Department of Chemistry, University of Cambridge, Cambridge, UK. [2]Cancer Research UK Cambridge Institute, University of Cambridge, Cambridge, UK. [3]School of Clinical Medicine, University of Cambridge, Cambridge, UK. [4]These authors contributed equally: Zutao Yu, Jochen Spiegel. e-mail: sb10031@cam.ac.uk

https://doi.org/10.1038/s41587-022-01636-0

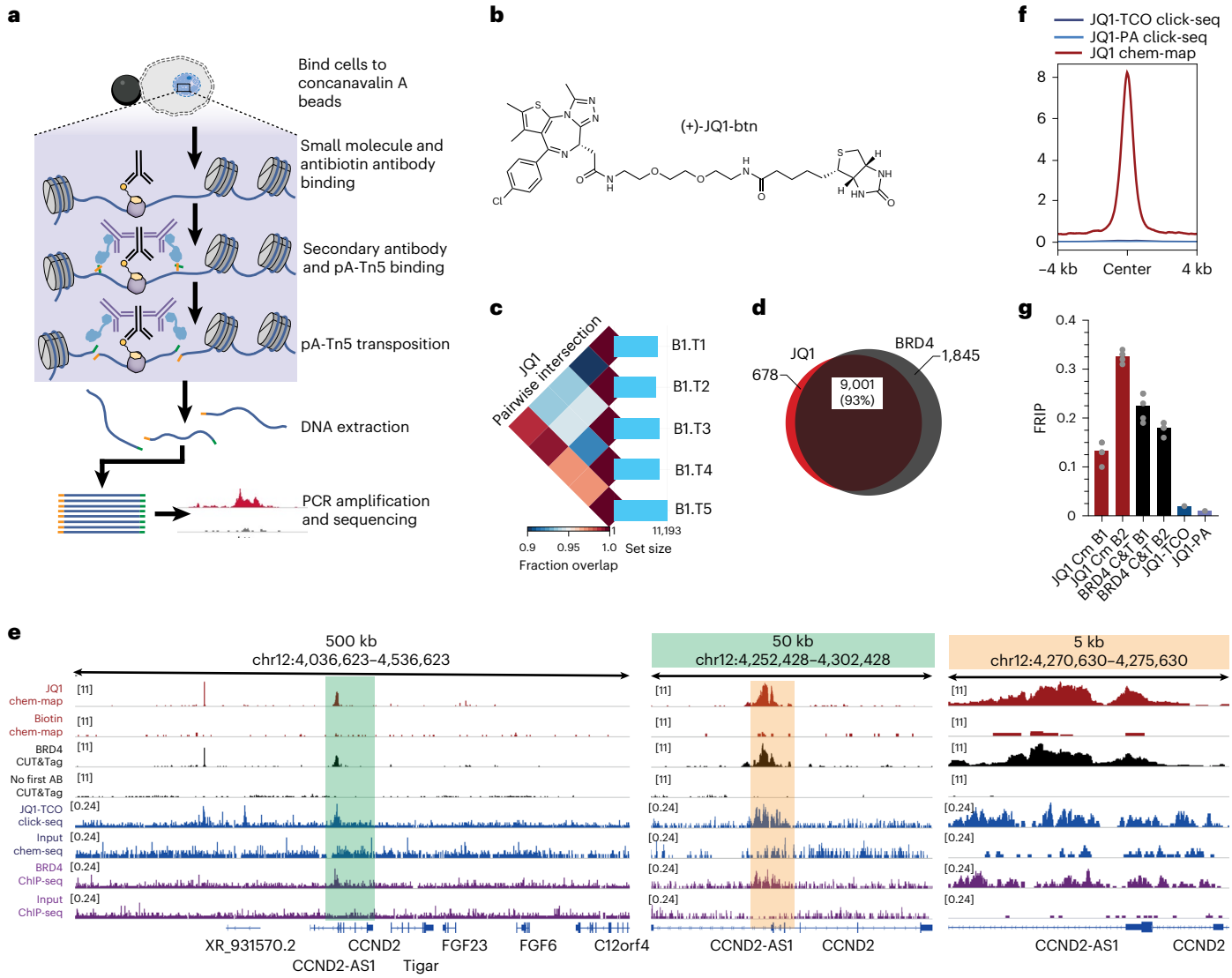

Fig. 1 | Chem-map reveals genomic binding sites for the BET bromodomain-targeting drug JQ1. a, Chem-map workflow—in permeabilized cells, a precomplex of biotinylated small molecules (yellow) and antibiotin antibody (black) bind to the chromatin target (protein or DNA). Then a secondary antibody (purple) tethering of pA–Tn5 transposomes (light blue) was recruited to the drug binding sites. Addition of Mg^{2+} activates the transposomes and integrates adapters (green and orange) in the proximity of the drug-binding sites. After DNA purification, genomic fragments with adapters at both ends are enriched via PCR, which allows the genome-wide identification of drug-binding sites by next-generation sequencing. **b**, Chemical structure of biotinylated JQ1. **c**, Pairwise intersection of enriched peaks across five technical replicates (T1–T5) in a biological replicate (B1) of K562 cells. **d**, Venn diagram illustrating the overlap of high-confidence binding sites of JQ1 (Chem-map, red) and its protein target BRD4 (CUT&Tag, black) in K562 cells. **e**, Genome browser views of JQ1 Chem-map (red), biotin negative control (red) and BRD4 CUT&Tag (black) and its negative control without adding primary antibody (first Ab), compared to published JQ1 Click-Chem-seq (blue) and BRD4 ChIP–seq (purple) data at the *CCND2* gene locus. Green and orange boxes highlight regions of respective close-up views. **f**, FRiP analysis comparing JQ1 Chem-map (Cm, $n = 5$), BRD4 CUT&Tag (C&T, $n = 5$), JQ1 Click-Chem-seq (Click-seq, different JQ1 derivatives JQ1-TCO and JQ1-PA, $n = 1$) and BRD4 ChIP–seq in K562 cells. **g**, Comparison of JQ1 Chem-map and published JQ1 Click-Chem-seq signal averaged at highest-confidence loci detected with BRD4 CUT&Tag in K562 cells. All sequencing data are normalized by sequencing depth.

DNA or chromatin-associated proteins. We illustrate the method with three distinct interaction modalities for molecules that either target a chromatin protein, a DNA secondary structure or intercalate DNA.

Results

Chem-map of a small-molecule–chromatin protein interaction

In the Chem-map approach, a covalent affinity tag is introduced to the small molecule and exploited to recruit a transposase (Tn5) to the binding site, followed by marking the site via proximal transposition events (Fig. 1a). Tn5 recruitment to proteins has been deployed in TAM-ChIP and CUT&Tag[15]. We introduced a preassembled complex, comprising a biotinylated small molecule together with antibiotin primary antibody, directly into permeabilized cells enabling the small molecule to bind the target. An anti-Ig secondary antibody precomplexed with a protein A–Tn5 fusion, loaded with sequencing adapters, is then incubated with the cells. Activation of the transposome with magnesium ions then triggers the insertion of sequencing adapters proximal to the small-molecule-binding sites. Tagmented DNA fragments that mark the small-molecule-binding sites are then extracted, selectively amplified, sequenced and mapped by alignment of sequenced reads to the genome.

We validated Chem-map for the BET inhibitor JQ1 in human leukemia K562 cells, as JQ1 interactions have been characterized using Click-Chem-seq in the same cell line[5]. In parallel, we mapped the genome-wide binding sites of the inhibitor's main target BRD4 using a

https://doi.org/10.1038/s41587-022-01636-0

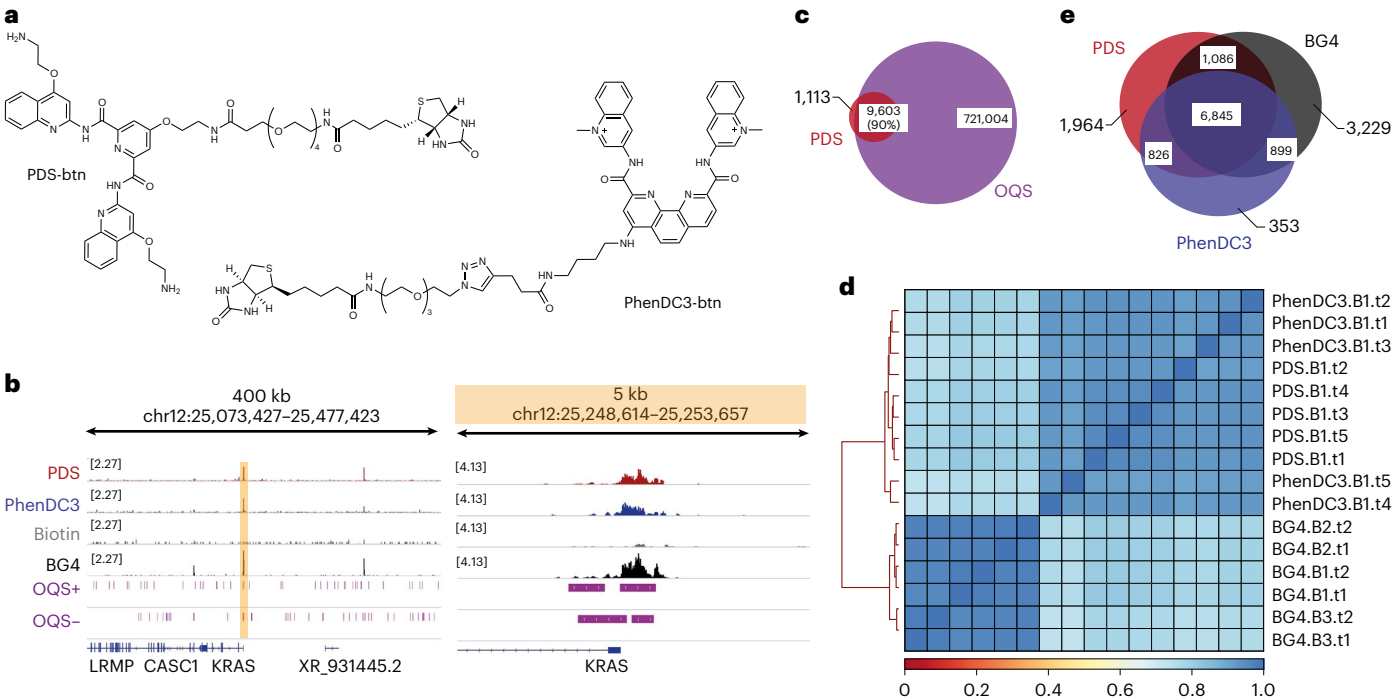

Fig. 2 | Chem-map reveals genomic binding sites of DNA G-quadruplex binding molecules in human K562 cells. a, Chemical structure of biotinylated G4 ligands PDS and PhenDC3. **b**, Genome browser views of Chem-map for PDS (red) and PhenDC3 (blue) compared to CUT&Tag data for the G4 antibody BG4 (black) at the *KRAS* locus. Sites that fold into G4 structures in vitro (OQs) are highlighted in purple for the plus and minus strands. The orange box highlights the regions of a close-up view. **c**, Venn diagrams illustrating the overlap of binding sites for the G4 ligand PDS and OQs. **d**, Hierarchical clustering of the Spearman correlation matrix for PDS Chem-map, PhenDC3 Chem-map and BG4 CUT&Tag. **e**, Venn diagrams illustrating the overlap of binding sites for the G4 ligands PDS and PhenDC3 and BG4.

specific antibody and the CUT&Tag approach[15]. Chem-map experiments were performed with the biotinylated derivative JQ1-btn (Fig. 1b) and biotin to control for background binding of the pA–Tn5 complex. We performed two biological replicates, each with five technical replicates, to evaluate the robustness and technical reproducibility of our approach (Supplementary Table 1). In each experiment, we observed around 10,000 JQ1 binding sites and high reproducibility of Spearman correlation $r_S > 0.77$ across replicates (Fig. 1c and Extended Data Fig. 1a,b). Next, we compared high-confidence JQ1 binding sites (Methods) obtained via Chem-map with BRD4 sites obtained via CUT&Tag and found 93% of JQ1 peaks overlap with BRD4 sites (Fig. 1d). Principal components analysis (PCA) confirmed that JQ1 and BRD4 data cluster together and are separated qualitatively from the biotin control (Extended Data Fig. 1c). Thus, Chem-map accurately captures JQ1 binding in cells. Similar observations were made in parallel experiments using the human osteosarcoma epithelial U2OS cells (Extended Data Fig. 1d).

We quantitatively compared the data quality of Chem-map to the published JQ1 Click-Chem-seq data in K562 cells[5]. Chem-map exhibited improved raw data quality yielding ~20-fold higher fraction of reads in peaks (FRiP) compared to Click-Chem-seq and is similar to CUT&Tag (Fig. 1e,f). We also plotted the average read counts for Chem-map and Click-Chem-seq around the highest-confidence BRD4 binding sites obtained by BRD4 CUT&Tag. Chem-map provided ~150-fold higher signal accumulation compared to Click-Chem-seq (maximum mean read count 8.17 counts per million (cpm) and 0.05 cpm, respectively) (Fig. 1g). This improvement in signal quality was observed while using 1×10^5 cells per experiment in Chem-map.

In situ mapping of DNA G-quadruplex binding

We next sought to map the binding sites of two structurally distinct DNA G-quadruplex (G4) recognizing molecules, pyridostatin (PDS) and PhenDC3 (Fig. 2a)[16,17]. G4s are four-stranded secondary structures that can form in G-rich DNA sequences. They have been detected in human cells and tissues and mapped in human chromatin using antibody approaches[18,19]. G4s have been implicated in gene regulation, cell fate transitions, and cancers and are under investigation as therapeutic targets for small-molecule drugs[20]. For instance, the G4 ligand PDS has been shown to modulate transcription, cause replication stalling and induce particular patterns of DNA damage[7]. There is a pressing need for a methodology to confirm that such molecules actually bind to G4 targets in situ and to elucidate those binding sites in different biological contexts. This is particularly relevant as the endogenous landscape of cellular G4 that are detectable appears to be only a small fraction of possible G4s in the genome[18]. Attempts to directly map the binding sites of G4 ligands in cells have been unsuccessful. Enrichment sequencing via pull-down of isolated genomic DNA only provided evidence of ligand binding to repetitive telomeric elements[21]. Indirect evidence has arisen from mapping surrogates such as γH2AX sites in the region of strand breaks caused by the binding events of G4 ligand PDS[7]. A likely limitation is small-molecule dissociation from the DNA target by physical separation during washing steps leading to low recovery and poor signal. Indeed, single-molecule imaging studies have shown that ligand binding lifetime to G4s in live cells is in the order of seconds[22]. We reasoned that a transposome-based method (Fig. 1a) might detect dynamic, noncovalent DNA–small-molecule interactions where the lifetime is sufficient for catalytic adapter insertion in situ.

Biotinylated G4 ligands PDS-btn and PhenDC3-btn were synthesized with a flexible, long PEG4 linker to minimize steric hindrance to recognition of the antibody binding and subsequent targeted DNA tagmentation (Fig. 2a). A fluorescence resonance energy transfer (FRET)-melting assay was employed to validate the binding of the

https://doi.org/10.1038/s41587-022-01636-0

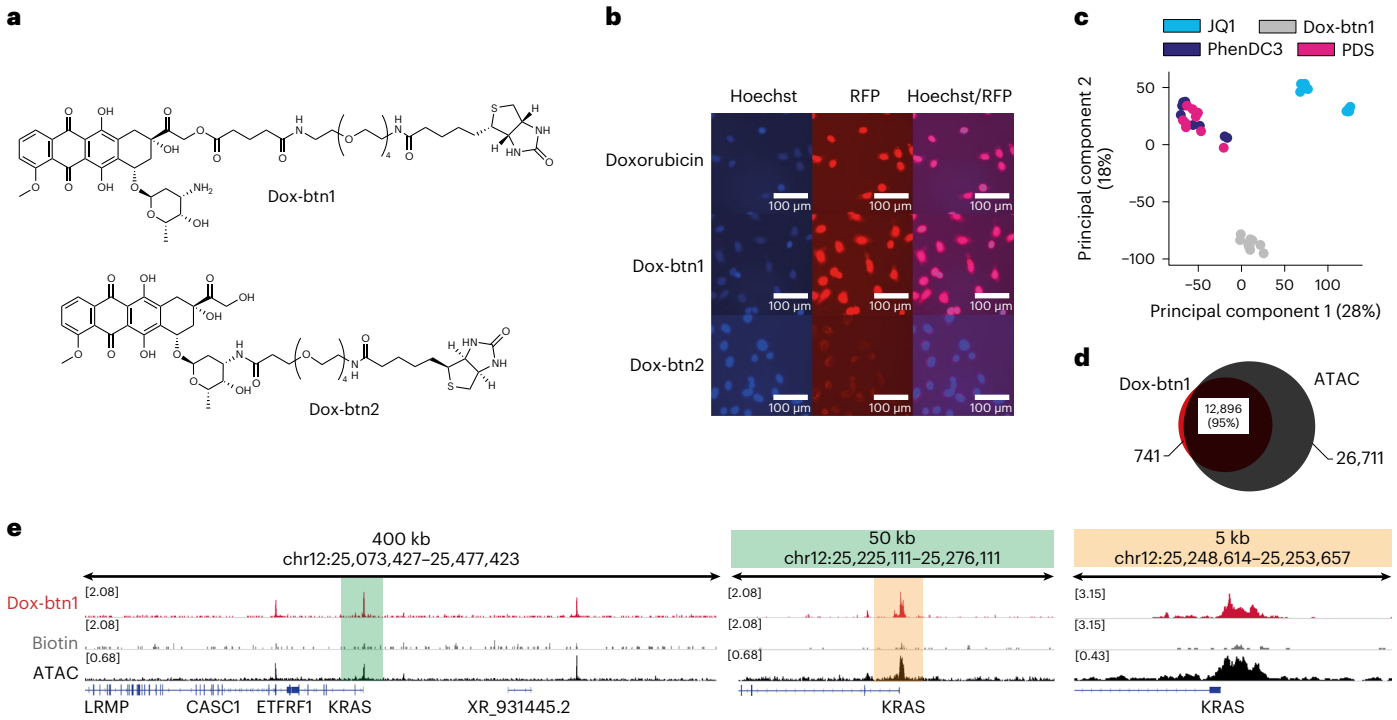

Fig. 3 | Chem-map reveals an open chromatin binding preference for doxorubicin. a, Chemical structure of biotinylated derivatives of doxorubicin. **b**, Microscopy analysis of U2OS cells visualizing nuclear enrichment of doxorubicin derivatives. Live U2OS cells were treated with doxorubicin and its derivatives for 6 h. Nuclei were stained with Hoechst 33342. BFB was used for visualization of nuclei (blue) and RFB was used for visualization of doxorubicin and its derivatives (red). Scale bar, 100 µm. Experiments were repeated independently three times. **c**, PCA analysis showing the distinct binding profiles of small molecules that have different protein and DNA targets in K562 cells. **d**, Venn diagram showing the overlap of doxorubicin binding sites with open chromatin mapped by ATAC-seq. **e**, Genome browser views of doxorubicin Chem-map binding sites (red) compared to a biotin control (gray) and ATAC-seq (black). BFB, blue-light filter cube; RFB, red-light filter cube.

tagged G4 ligands to different G4s (Extended Data Fig. 2a and Supplementary Tables 2 and 3). We employed both PDS-btn and PhenDC3-btn in our Chem-map protocol in K562 cells, employing biotin as a negative control and performing two biological replicates each with five technical replicates. For both G4 ligands, we obtained high-quality maps revealing about 10,000 high-confidence binding sites for each of the two G4 ligands (Fig. 2b). It was gratifying to observe that PDS and PhenDC3 binding sites showed considerable overlap (90% for PDS and 76% for PhenDC3, respectively) with where G4s can potentially form experimentally observed G-quadruplexes (OQs) based on G4-sensitive sequencing (G4-seq) of purified human genomic DNA (Fig. 2c and Extended Data Fig. 2b)[23]. We also compared the small-molecule-binding sites to maps of endogenous G4s detected in chromatin using the G4 antibody BG4 (Fig. 2d)[24]. We observed a strong overlap of high-confidence binding sites (Fig. 2e) and signal correlation when comparing BG4 antibody and G4 ligands with Spearman correlations (r_s) of 0.74 and 0.87 for PDS and PhenDC3, respectively (Fig. 2d). Similarly, differential binding analysis revealed that PDS and PhenDC3 bind primarily to the same cellular G4 sites (Extended Data Fig. 2c). Notably, PCA analysis confirmed clear qualitative separation of the biotinylated probes from the biotin control experiments confirming that signal enrichment is caused by the small molecule rather than nonspecific interactions of Tn5 (Extended Data Fig. 2d). To rule out potential fixation artifacts[25], we repeated PDS Chem-map in unfixed K562 cells observing an overall consistent peak distribution (~10,000 high-confidence peaks, 88% in the OQs and 75% overlap with binding sites in gently fixed K562 cells) (Extended Data Fig. 2e,f). Furthermore, to confirm that Chem-map reflects small-molecule-binding sites in live cells, we treated K562 cells with unmodified PDS (4 µM for 3 h) before PDS Chem-map (Extended Data Fig. 2g–i). We observed a drop in recovered DNA material and a considerable reduction in peak numbers (~6,000 sites (60%) lost compared to untreated).

These data obtained within human cells confirm that PDS, PhenDC3 and BG4 are specific to the G4 family of DNA structures and capable of binding a variety of G4 sequences and structural sub-types, consistent with biophysical studies[18,23]. Notably, the small-molecule Chem-map data provide vital cross-validation of cellular G4 sites previously detected using the BG4 antibody.

Chem-map reveals landscape of doxorubicin–DNA interactions

We evaluated the interactions of the clinically approved drug doxorubicin, which is thought to act by targeting DNA but has not yet been directly mapped to genomic DNA in cells. Doxorubicin belongs to the anthracycline class of antitumor antibiotics. Anthracyclines are generally considered to be DNA intercalators that can inhibit the action of topoisomerase II and can form reactive hydroxyl radicals proximal to DNA, leading to DNA damage and cellular cytotoxicity[1]. Around 1 million cancer patients annually receive treatment with doxorubicin or its variants. However, despite much research and clinical use over five decades, its molecular mode of action is, somewhat surprisingly, still not well understood[26].

For Chem-map, it was necessary to design an appropriately tagged derivative of doxorubicin. We evaluated two points of conjugation to doxorubicin at 14-OH and 3′-NH_2 resulting in biotinylated derivatives Dox-btn1 and Dox-btn2, respectively (Fig. 3a). Next, we examined the cellular distribution in U2OS cells using fluorescence microscopy utilizing the intrinsic fluorescence of doxorubicin (Fig. 3b). Notably, doxorubicin and Dox-btn1 were predominantly accumulated in the nuclei, whereas Dox-btn2 was mainly located in the cytoplasm, in agreement

https://doi.org/10.1038/s41587-022-01636-0

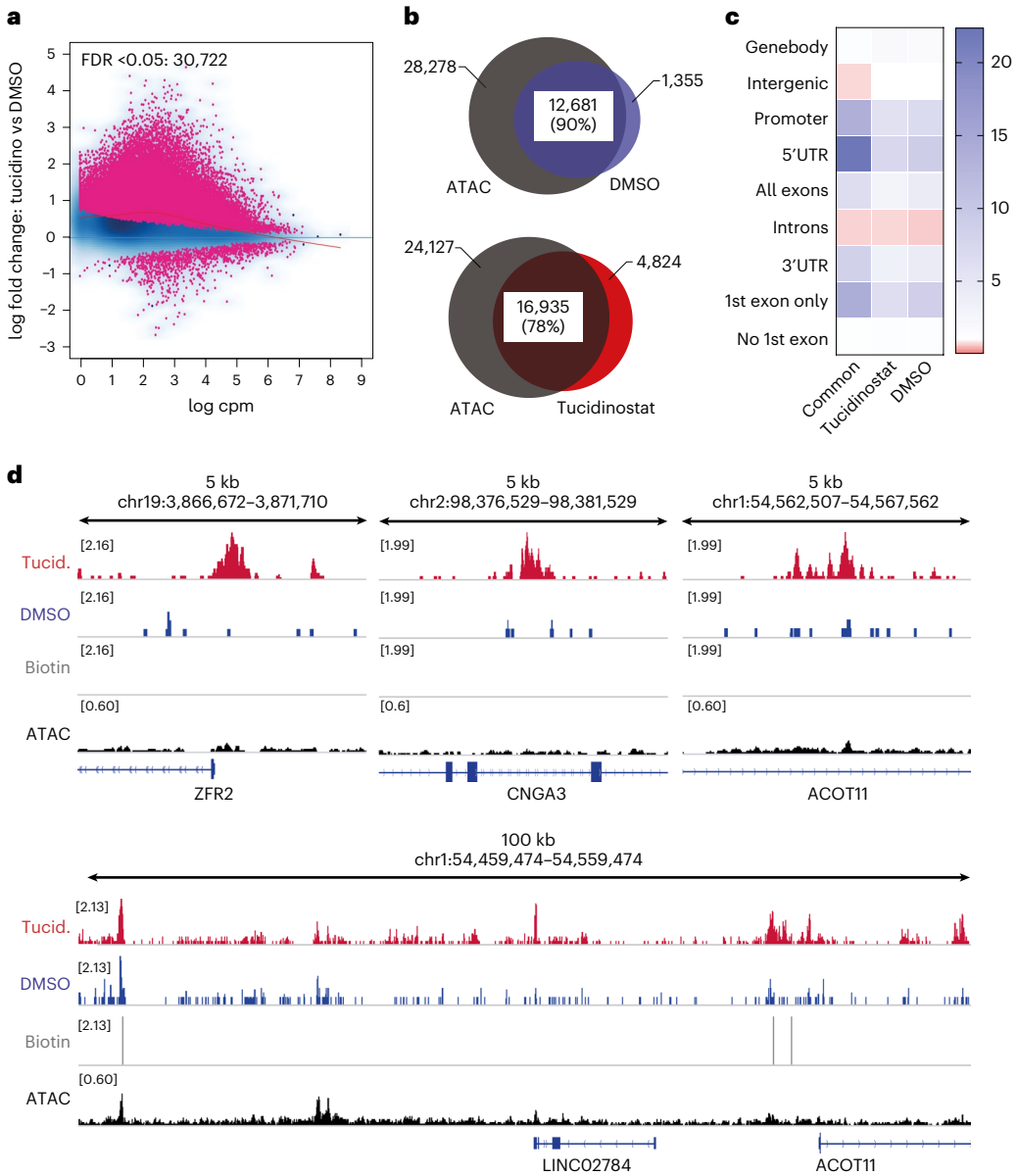

Fig. 4 | Chem-map reveals response to drug combinations. a, Differential binding analysis showing differences in Dox-btn1 Chem-map peaks for tucidinostat-treated (1 µM, 72 h) and vehicle-treated (0.1% DMSO, 72 h) K562 cells. Red dots represent sites where the binding is substantially different (FDR < 0.05) for two treatments (considering three biological replicates each with five technical replicates). A positive fold change indicates an increase in Dox-btn1 binding. **b**, Venn diagram illustrating the overlap of high-confidence Dox-btn1 binding sites with ATAC-seq in vehicle-treated (blue) and tucidinostat-treated (red) K562 cells. **c**, Enrichment over random (n = 1,000 permutations) of Dox-btn1 Chem-map peaks at genomic features from the reference human annotation GENECODE v.28. Up/down, substantially up- or down-regulated peaks in tucidinostat-treated K562 cells. Promoter defined as 1 kb upstream transcription start sites. **d**, Genome browser views displaying the difference in Dox-btn1 binding for tucidinostat-treated (red) or vehicle-treated (blue) cells in K562 cells compared to a biotin control (gray) and ATAC-seq (black). UTR, untranslated region.

with a previous study[27]. Negligible amounts of DNA were recovered using Chem-map with Dox-btn2 in K562 cells, whereas Dox-btn1 recovered substantial amounts of DNA (Extended Data Fig. 3a), consistent with its nuclear localization.

Biophysical experiments show that doxorubicin intercalates double-stranded DNA preferentially at a GC base pair[28], which does not in itself inform genomic binding sites. Chem-map data from two biological and five technical replicates in K562 cells revealed 14,000 high-confidence Dox-btn1 binding sites (Fig. 3e and Extended Data Fig. 3b), with an excellent signal-to-noise ratio (Extended Data Fig. 3c). We compared Dox-btn1 binding sites to the binding sites of JQ1, PDS and PhenDC3, each measured by Chem-map. Both PCA (Fig. 3c) and differential binding analyses (Extended Data Fig. 3d) revealed distinct binding profiles for the three types of ligands, caused by the different target binding modalities for the respective probes. The 14,000 doxorubicin peaks were predominantly (95%) in open chromatin regions, as defined by ATAC-seq[29] (Fig. 3d,e). Given that Tn5-based approaches can map features in both euchromatin and heterochromatin[15], enrichment of Dox-btn1 at open chromatin is unlikely to be an artifact of Tn5 accessibility. Notably, we found Dox-btn1 binding sites particularly enriched at promoters and 5′-untranslated regions (Extended Data Fig. 3e), which helps explain why doxorubicin preferentially induces DNA double-strand breaks near promoters[30].

HDACi sensitizes cancer to doxorubicin by augmenting binding

The dynamic nature of chromatin status makes it difficult to predict and control the response to chromatin-targeted drugs in cells[4]. Chem-map enables the measurement of changes in drug binding profiles to help understand the mode of action and optimize their deployment. To exemplify this, we applied Chem-map to measure how epigenetic modulators can enhance DNA–drug interaction to create drug synergy. Specifically, we investigated how doxorubicin binding in cells changes upon treatment with a histone deacetylases inhibitor (HDACi). Histone deacetylases (HDAC) are key chromatin modifiers and commonly dysregulated in cancers, making them promising therapeutic targets for cancer. Preclinical and clinical studies show that HDAC inhibition can sensitize the response of cancer to doxorubicin treatment[31,32]. We chose to use tucidinostat (chidamide), a selective inhibitor of class I HDAC1–HDAC3 and class IIb HDAC10, which has been clinically approved for peripheral T-cell lymphoma and adult T-cell leukemia-lymphoma[33,34]. Preclinical and clinical trials of tucidinostat in combination with doxorubicin are ongoing[35] (NCT04231448). We treated K562 leukemia cells with tucidinostat (1 µM) for 72 h, followed by Chem-map with Dox-btn1. From three biological replicates, each with five technical replicates, we observed excellent reproducibility and clear separation of tucidinostat treatment and vehicle control (Extended Data Fig. 4). Tucidinostat treatment resulted in a substantial shift in Dox-btn1 binding events (30,722 substantially changing sites), mainly comprising stronger binding events and new binding sites, as judged by differential binding analysis (Fig. 4a,d). More doxorubicin binding events were detected at sites that had originally exhibited closed chromatin in the absence of tucidinostat treatment (22% in tucidinostat compared with 10% in vehicle group), consistent with considerable chromatin remodeling (Fig. 4b). In addition, new peaks observed following tucidinostat treatment were mainly located at promoters and 5′-untranslated regions (Fig. 4c,d). Thus, HDAC inhibitors likely sensitize cancer cells via expanding existing drug-binding sites and establishing new interaction sites to enhance the overall volume of drug–target interactions. These molecular data explain clinically relevant drug synergistic effects[31,32].

Discussion

There is a considerable demand for a robust and general approach to map the interaction between small molecules and chromatin in situ. Small molecules can target chromatin in ways that interfere with vital processes that include DNA replication, transcription, DNA repair, DNA and histone modifications, and epigenetic reprogramming, which has also led to therapeutic drugs. In this study, we show that Chem-map is a robust approach for mapping the interactions of small molecules with genomic DNA and chromatin proteins in cells. Chem-map provides unprecedented signal quality and has generated insights into the genomic targeting of probe molecules and also a clinically relevant drug, which was previously not attainable. Therefore, we expect that Chem-map can be adapted to a wide range of chromatin-interacting molecules and studies involving low cell numbers and rare epitopes. Nonetheless, probe concentrations will have to be titrated depending on the abundance of binding sites and strength of the interaction (also see Supplementary Technical Discussion). For instance, we observed substantially stronger enrichment for the intercalator doxorubicin compared to the protein binder JQ1 or the DNA G4 binding ligands. While gentle formaldehyde fixation is commonly used to avoid decomposition or clumping of permeabilized cells during the protocol[36] and can be omitted in certain cases (see for example PDS Chem-map), fixation becomes relevant when small-molecule probes directly compete for chromatin binding domains of the target proteins. In these cases, formaldehyde concentrations and cross-linking times should be titrated to allow for efficient recovery, while still limiting fixation artifacts such as epitope masking[25]. In addition, the attachment of the biotin linker will have to be performed such that small-molecule target binding is not impaired and will either require an intricate understanding of the underlying structure–activity relationship or the synthesis of various derivatives (Fig. 3a). Ideally, this process should be guided by some form of functional (Fig. 3b) or biophysical validation of the tagged molecule (Extended Data Fig. 2). Notably, the exploration of suitable linker positions for a variety of small-molecule probes and drugs has considerably increased due to their application in other therapeutic platforms such as antibody-drug conjugates[37] or proteolysis targeting chimeras[38].

In addition to the direct mapping of native binding sites, we have shown that Chem-map is able to capture the dynamics of drug binding under changing cellular conditions. We provide a molecular explanation as to how chromatin modulation by epigenetic drugs can enhance the targeting of genomic DNA and sensitize cancer cells to DNA-damaging agents. This is in line with previous observations that cotreatment of a cisplatin derivative with the HDAC inhibitor SAHA or the DNA methyl transferase inhibitor azacytidine activate DNA damage response pathways and increase DNA lesions[39].

Chem-map will complement other genomics techniques to enable mechanistic studies and further development of genome- and epigenome-targeting drugs.

Online content

Any methods, additional references, Nature Portfolio reporting summaries, source data, extended data, supplementary information, acknowledgements, peer review information; details of author contributions and competing interests; and statements of data and code availability are available at https://doi.org/10.1038/s41587-022-01636-0.

References

1. Silverman, R.B. & Holladay, M.W. *The Organic Chemistry of Drug Design and Drug Action Third Edition* (Elsevier, 2014).
2. Schenone, M., Dančík, V., Wagner, B. K. & Clemons, P. A. Target identification and mechanism of action in chemical biology and drug discovery. *Nat. Chem. Biol.* **9**, 232–240 (2013).
3. Anders, L. et al. Genome-wide localization of small molecules. *Nat. Biotechnol.* **32**, 92–96 (2014).
4. Rodriguez, R. & Miller, K. M. Unravelling the genomic targets of small molecules using high-throughput sequencing. *Nat. Rev. Genet.* **15**, 783–796 (2014).
5. Tyler, D. S. et al. Click chemistry enables preclinical evaluation of targeted epigenetic therapies. *Science* **356**, 1397–1401 (2017).
6. Jin, C. et al. Chem-seq permits identification of genomic targets of drugs against androgen receptor regulation selected by functional phenotypic screens. *Proc. Natl Acad. Sci. USA* **111**, 9235–9240 (2014).
7. Rodriguez, R. et al. Small-molecule-induced DNA damage identifies alternative DNA structures in human genes. *Nat. Chem. Biol.* **8**, 301–310 (2012).
8. Vaughn, C. M., Selby, C. P., Yang, Y., Hsu, D. S. & Sancar, A. Genome-wide single-nucleotide resolution of oxaliplatin-DNA adduct repair in drug-sensitive and -resistant colorectal cancer cell lines. *J. Biol. Chem.* **295**, 7584–7594 (2020).
9. Sutormin, D., Rubanova, N., Logacheva, M., Ghilarov, D. & Severinov, K. Single-nucleotide-resolution mapping of DNA gyrase cleavage sites across the *Escherichia coli* genome. *Nucleic Acids Res.* **47**, 1373–1388 (2018).
10. Shu, X., Xiong, X., Song, J., He, C. & Yi, C. Base-resolution analysis of cisplatin-DNA adducts at the genome scale. *Angew. Chem. Int. Ed. Engl.* **55**, 14246–14249 (2016).
11. Gittens, W. H. et al. A nucleotide resolution map of Top2-linked DNA breaks in the yeast and human genome. *Nat. Commun.* **10**, 4846 (2019).
12. Meier, J. L., Yu, A. S., Korf, I., Segal, D. J. & Dervan, P. B. Guiding the design of synthetic DNA-binding molecules with massively parallel sequencing. *J. Am. Chem. Soc.* **134**, 17814–17822 (2012).

13. Anandhakumar, C. et al. Next-generation sequencing studies guide the design of pyrrole-imidazole polyamides with improved binding specificity by the addition of beta-alanine. *ChemBioChem* **15**, 2647–2651 (2014).
14. Erwin, G. S. et al. Synthetic genome readers target clustered binding sites across diverse chromatin states. *Proc. Natl. Acad. Sci. USA* **113**, E7418–E7427 (2016).
15. Kaya-Okur, H. S. et al. CUT&Tag for efficient epigenomic profiling of small samples and single cells. *Nat. Commun.* **10**, 1930 (2019).
16. Rodriguez, R. et al. A novel small molecule that alters shelterin integrity and triggers a DNA-damage response at telomeres. *J. Am. Chem. Soc.* **130**, 15758–15759 (2008).
17. De Cian, A., Delemos, E., Mergny, J. L., Teulade-Fichou, M. P. & Monchaud, D. Highly efficient G-quadruplex recognition by bisquinolinium compounds. *J. Am. Chem. Soc.* **129**, 1856–1857 (2007).
18. Hänsel-Hertsch, R. et al. G-quadruplex structures mark human regulatory chromatin. *Nat. Genet.* **48**, 1267 (2016).
19. Biffi, G., Tannahill, D., McCafferty, J. & Balasubramanian, S. Quantitative visualization of DNA G-quadruplex structures in human cells. *Nat. Chem.* **5**, 182–186 (2013).
20. Spiegel, J., Adhikari, S. & Balasubramanian, S. The structure and function of DNA G-quadruplexes. *Trends Chem.* **2**, 123–136 (2020).
21. Müller, S., Kumari, S., Rodriguez, R. & Balasubramanian, S. Small-molecule-mediated G-quadruplex isolation from human cells. *Nat. Chem.* **2**, 1095–1098 (2010).
22. Di Antonio, M. et al. Single-molecule visualization of DNA G-quadruplex formation in live cells. *Nat. Chem.* **12**, 832–837 (2020).
23. Chambers, V. S. et al. High-throughput sequencing of DNA G-quadruplex structures in the human genome. *Nat. Biotechnol.* **33**, 877 (2015).
24. Hui, W. W. I., Simeone, A., Zyner, K. G., Tannahill, D. & Balasubramanian, S. Single-cell mapping of DNA G-quadruplex structures in human cancer cells. *Sci Rep.* **11**, 23641 (2021).
25. Baranello, L., Kouzine, F., Sanford, S. & Levens, D. ChIP bias as a function of cross-linking time. *Chromosome Res.* **24**, 175–181 (2016).
26. Qiao, X. et al. Uncoupling DNA damage from chromatin damage to detoxify doxorubicin. *Proc. Natl Acad. Sci. USA* **117**, 15182–15192 (2020).
27. Di Meo, C. et al. Polyaspartamide-doxorubicin conjugate as potential prodrug for anticancer therapy. *Pharm. Res.* **32**, 1557–1569 (2015).
28. Frederick, C. A. et al. Structural comparison of anticancer drug-DNA complexes: adriamycin and daunomycin. *Biochemistry* **29**, 2538–2549 (1990).
29. Shen, J. et al. Promoter G-quadruplex folding precedes transcription and is controlled by chromatin. *Genome Biol.* **22**, 143 (2021).
30. Yang, F., Kemp, C. J. & Henikoff, S. Anthracyclines induce double-strand DNA breaks at active gene promoters. *Mutat. Res.* **773**, 9–15 (2015).
31. Munster, P. N. et al. Phase I trial of vorinostat and doxorubicin in solid tumours: histone deacetylase 2 expression as a predictive marker. *Br. J. Cancer* **101**, 1044–1050 (2009).
32. Vu, K. et al. Romidepsin plus liposomal doxorubicin is safe and effective in patients with relapsed or refractory T-cell lymphoma: results of a phase I dose-escalation study. *Clin. Cancer Res.* **26**, 1000–1008 (2020).
33. Pan, D. et al. Discovery of an orally active subtype-selective HDAC inhibitor, chidamide, as an epigenetic modulator for cancer treatment. *MedChemComm* **5**, 1789–1796 (2014).
34. Shi, Y. et al. Results from a multicenter, open-label, pivotal phase II study of chidamide in relapsed or refractory peripheral T-cell lymphoma. *Ann. Oncol.* **26**, 1766–1771 (2015).
35. Zhang, M. et al. Clinical efficacy and molecular biomarkers in a phase II study of tucidinostat plus R-CHOP in elderly patients with newly diagnosed diffuse large B-cell lymphoma. *Clin. Epigenetics* **12**, 160 (2020).
36. Kaya-Okur, H. S., Janssens, D. H., Henikoff, J. G., Ahmad, K. & Henikoff, S. Efficient low-cost chromatin profiling with CUT&Tag. *Nat. Protoc.* **15**, 3264–3283 (2020).
37. Beck, A., Goetsch, L., Dumontet, C. & Corvaïa, N. Strategies and challenges for the next generation of antibody-drug conjugates. *Nat. Rev. Drug Discov.* **16**, 315–337 (2017).
38. Li, K. & Crews, C. M. PROTACs: past, present and future. *Chem. Soc. Rev.* **51**, 5214–5236 (2022).
39. Zacharioudakis, E. et al. Chromatin regulates genome targeting with cisplatin. *Angew. Chem. Int. Ed.* **56**, 6483–6487 (2017).

Methods

Cell culture and compound treatment

Mycoplasma-free human chronic myelogenous leukemia K562 cells (RRID:CVCL 0004) were purchased from ATCC and cultured in RPMI 1640 (Gibco, 21875034) supplemented with 10% heat-inactivated FBS (Gibco, A3840401). Human bone osteosarcoma epithelial U2OS cells (RRID:CVCL_0042) derived from a moderately differentiated sarcoma were obtained from ATCC and cultured in DMEM (Gibco, 41966029) supplemented with 10% FBS. Both cell lines were grown in accordance with ENCODE cell culture protocols and tested for mycoplasma contamination and identity confirmed by STR typing.

HDAC inhibitor tucidinostat (also named as Chidamide/HBI-8000/CS-055; Sellect, S8567) was prepared at 10 mM as stock solution in DMSO. Cells were treated with tucidinostat dissolved to 1 μM final concentration or an equal concentration of vehicle (0.1% DMSO) for 72 h.

FRET melting assay

A total of 400 nM fluorescein (FAM)-5-carboxytetramethylrhodamine dual-labeled oligonucleotides (Biomers; see Supplementary Table 1) was annealed in FRET assay buffer (60 mM potassium cacodylate, pH = 7.4) at 95 °C for 5 min, followed by gradually cooling down to 20 °C. A series of probe concentrations were prepared in an 8-well strip tube as follows: 150 μl of 6 μM ligand in assay buffer was prepared as the initial concentration. Subsequent serial dilutions were made by adding 100 μl of probe solutions to 50 μl of assay buffer, resulting in 12 concentrations, including a control (1% DMSO). A total of 25 μl per solution was transferred to a 96-well plate, followed by adding 25 μl of annealed oligonucleotide solutions to each well. The plate was then sealed with an adhesive transparent cover and shaken gently for 10 min at room temperature. Measurements of restoring FAM signal were recorded on a real-time PCR detection system (Bio-Rad, CFX96) employing a temperature gradient from 25 °C to 95 °C at 0.5 °C min^{-1}. Melting temperatures (T_m) were determined by the first derivative maxima of relative fluorescence unit value against time, and ΔT_m was calculated by baseline correction of melting temperatures subtracting control group. A one-site binding model in GraphPad Prism 8 was used to fit FRET T_m curves. Mean was calculated from two replicates.

Cell imaging

U2OS cells were plated in a 12-well plate in DMEM medium supplemented with 10% FBS. After 18 h incubation, cells were treated for 6 h with doxorubicin (1 μM), Dox-btn1 (1 μM), Dox-btn2 (1 μM) and 0.1% DMSO (control), respectively, in fresh medium. Then cells were washed twice with PBS and lightly fixed with 0.1% formaldehyde for 2 min. Cells were then incubated with Hoechst 33,342 for 10 min at room temperature to label the cell nuclei. Imaging was captured in EVOS M5000 microscope (Thermo Fisher Scientific). Blue-light filter cube with wavelength of Exc 357/44 nm and Emi 447/60 nm was used for visualization of nuclei and red-light filter cube with wavelength of Exc 531/40 nm and Emi 593/40 nm was used for visualization of doxorubicin and its derivatives.

Chem-map protocol

Cell preparation. U2OS cells were detached using Accutase (Stem Cell Technologies, 07920) and quenched using complete culture media. U2OS and K562 cells were collected by centrifugation and fixed in 0.1% formaldehyde (Thermo Fisher Scientific, 28906) in PBS for 2 min at room temperature, followed by quenching with glycine (Sigma-Aldrich, 50046) to a final concentration of 75 mM. Fixed cells were collected by centrifugation at 600*g* for 4 min, followed by resuspension in cold wash buffer (20 mM HEPES, pH 7.5, 150 mM NaCl and 0.5 mM spermidine (Sigma-Aldrich, S0266)) in nuclease-free water supplemented with a complete protease inhibitor, EDTA-free (Sigma-Aldrich, 11873580001). (Note: For Chem-map of G4 ligands, NaCl was replaced by equivalent concentrations of KCl in all buffers to maintain G4 stability. For optimal results, the concentration of cells needs to be adjusted based on target abundance and relative affinity of the probes. We employed cells at a concentration of 1,500 cells per μl (JQ1-btn) and 6,000 cells per μl (G4 ligands and biotinylated doxorubicin)).

Probe-1st Ab complex assembly. Compound stock solution in DMSO was diluted to 10 μM in antibody buffer (2 mM EDTA, 0.1% BSA (Sigma-Aldrich, A8577) and 0.05% digitonin (EMD Millipore, 300410) in wash buffer). For 5 samples, 20 μl probe solution (10 μM) and 16.7 μl antibiotin (D5A7) Rabbit mAb (Cell Signaling Technology, 5597; concentration is ~10 μM) was added to 200 μl antibody buffer and incubated on ice for 1 h to perform a complex at high concentration (probe in excess 1.2:1 to avoid nonspecific antibody binding). Next, 300 μl antibody buffer was added to the probe-1st Ab complexes solution. The final concentration of small molecule is 0.4 μM. (Note: For Dox-btn1, final concentration is diluted to 0.2 μM. For antibiotin antibody, dilution is 30×).

Bead capture. For five samples, 50 μl (for JQ1-btn) or 75 μl (for G4 ligands and biotinylated doxorubicin) concanavalin A beads (Bangs Labs, BP531) were washed twice in 1 ml binding buffer (20 mM HEPES, pH 7.5, 10 mM KCl, 1 mM $CaCl_2$ and 1 mM $MnCl_2$ in nuclease-free water) and resuspended in 75 μl binding buffer. A total of 100 μl of cell suspension was incubated with 10 μl prewashed concanavalin A beads at 25 °C for 10 min at 600 rpm. Beads-bound cells were gently washed twice with wash buffer before resuspending in 100 μl probe-1st Ab precomplex solution and incubating at 4 °C overnight at 600 rpm.

2nd Ab–Tn5 transposome complex assembly. pA–Tn5 assembled with DNA adapters were prepared as described in ref. [24]. For 5 samples, 2.5 μl 2nd Ab (Antibodies-Online, ABIN101961, ~8 μM) and 5 μl pA–Tn5 transposome (pA–Tn5 concentration is 2 μM) were added to 200 μl Dig-300 buffer (20 mM HEPES pH 7.5, 300 mM NaCl, 0.5 mM spermidine and 0.01% digitonin in nuclease-free water supplemented with complete protease inhibitor, EDTA-free) and incubated on ice for 1 h (2nd Ab and pA–Tn5 at a ratio of 2:1). A total of 300 μl antibody buffer was added to the 2nd–Tn5 complex solution.

Tagmentation. Cells were washed three times with 500 μl Dig-wash buffer (0.05% digitonin in wash buffer) and resuspended in 100 μl 2nd Ab–Tn5 transposome complex solution and incubated at 25 °C for 1 h at 600 rpm. Cells were then washed three times in 500 μl Dig-300 buffer before incubation in 300 μl tagmentation buffer (10 mM $MgCl_2$ in Dig-300 buffer) at 37 °C for 1 h at 600 rpm.

DNA extraction. After tagmentation, cells were washed twice with 500 μl TAPS wash buffer (10 mM (tris(hydroxymethyl) methylamino) propanesulfonic acid (TAPS; Alfa Aesar, J63268.AE), 0.2 mM EDTA in nuclease-free water). One hundred fifty microliters of extraction buffer (0.5 mg ml^{-1} proteinase K (Thermo Fisher Scientific, EO0491), 0.5% SDS (Sigma-Aldrich, L4509) in 10 mM Tris–HCl, pH 8.0) were added, vortexed and incubated at 55 °C for 1 h at 800 rpm. Next, 150 μl phenol–chloroform–isoamyl alcohol (Invitrogen, 15593049) was added and mixed. The mixture was transferred to MaXtract High-Density phase-lock tubes (QIAGEN, 129046) and centrifuged at room temperature for 3 min at 16,000*g*. A total of 150 μl chloroform was added to the top aqueous phase, mixed by inverting the phase-lock tubes for 10 times, and centrifuged 16,000*g* at room temperature for 3 min. The top aqueous layer was transferred to a 1.5 ml DNA Lo-bind tube (Eppendorf, 022431021). A total of 6 μl 5 M NaCl and 375 μl cold ethanol were added, mixed and incubated at −20 °C overnight. Samples were centrifuged at 21,130*g* at 4 °C for 30 min. The supernatant was carefully poured off and the DNA pellet rinsed with 1 ml cold 100% ethanol followed by centrifugation at 21,130*g* at 4 °C for 2 min. After pouring off the wash and draining the residual liquid with paper towel, the pellet was left

to air dry. Finally, the pellet was resuspended in 25 µl elution buffer 1 (10 mM Tris–HCl, pH 8, 1 mM EDTA, 1/400 RNAse A (Thermo Fisher Scientific, EN0531) in nuclease-free water) by vortexing and incubating at 37 °C for 10 min at 800 rpm.

Library preparation. In a 0.2 ml PCR tube, 25 µl NEBNext Ultra II Q5 2x PCR master mix (NEB, M0544), 2 µl of 10 µM uniquely barcoded v2 Ad1.x primer[40], 2 µl of 10 µM uniquely barcoded v2 Ad2.x primer[40] and 21 µl tagmented DNA were added and subjected to PCR (72 °C for 5 min, 98 °C for 30 s, followed by 10 cycles of 98 °C for 10 s and 63 °C for 10 s and one cycle of 72 °C for 1 min). Libraries were purified using 1.3× ratio (65 µl) Ampure XP beads (Beckman Coulter, A63882). After 10-min incubation at room temperature, bead-bound DNA was washed twice with 80% ethanol and libraries were eluted with 25 µl 10 mM Tris–HCl for 5 min at room temperature. (Note: PCR program condition for Dox-btn1 is 72 °C for 5 min, 98 °C for 2 min, followed by 10 cycles of 98 °C for 10 s and 63 °C for 10 s, and one cycle of 72 °C for 1 min, to maximally disrupt doxorubicin–DNA interaction.)

Library sequencing. Library size and concentration were measured using a TapeStation HSD1000 ScreenTape (Agilent, 5067–5584). Libraries were balanced and pooled for size selection using Ampure XP beads. 0.4× ratio of Ampure XP beads was added to pooled libraries and the supernatant transferred to a new tube after 15 min at room temperature. 1.3× ratio of Ampure XP beads was then added to the supernatant and incubated for 15 min at room temperature. Beads were washed twice with 80% ethanol and libraries eluted in 40 µl 10 mM Tris–HCl. Libraries were sequenced on a NextSeq 500 sequencer (Illumina) with a paired-end format of 36 bp × 2 using the High Output kit (Illumina, FC-404-2005).

CUT&Tag method

pA–Tn5 assembled with DNA adapters were prepared in the lab as described in ref. [24]. BRD4 CUT&Tag was performed as described before[36]. Briefly, cells were incubated with activated concanavalin A-coated magnetic beads (Bangs Labs, BP531). The bead-bound cells were permeabilized and incubated with anti-BRD4 (E2A7X) rabbit antibody (Cell Signalling Technology, 13440) in antibody buffer at a ratio of 1:50, followed by Guinea Pig anti-rabbit antibody (Antibodies-Online, ABIN101961) in Dig-wash buffer at a ratio of 1:100. Diluted pA–Tn5 adapter complex (1:250 ratio) was then added in Dig-300 buffer followed by the tagmentation reaction in tagmentation buffer. Extracted DNA fragments were used for library preparation and Illumina sequencing.

Sequencing data processing

Data demultiplexing and deduplication. Illumina sequencing paired-end output files were demultiplexed using demuxIllumina version 3.0.9 using the flags; -c -d -i -e -t 1 -r 0.01 -R -l 9. The resulting fq.gz files underwent sequencing quality control using FastQC version 0.11.8, and their summary was visualized by MultiQC version 1.11. Bases with a quality score below 20 were trimmed from both reads using cutadapt (cutadapt -q 20). Fastq files were aligned to the combined hg38 and *Escherichia coli* (*E. coli*) genomes using bwa version 0.7.17-r1188 with only reads in the whitelist regions of hg38 continuing the process pipeline. Duplicates were removed using Picard version 2.20.3 (Picard MarkDuplicates). Peaks were called using Seacr version 1.3 without input control reporting the top 1% by AUC regions, using both the relaxed and stringent criteria. BigWig files were created on the demultiplexed BAM file, normalized at cpm using deepTools version 2.0.

Consensus regions and reference comparisons. To address the ambiguity of peak calling, multiple approaches have been used to assess the peak number and overlaps between experiments. Namely, further thresholds have been applied on the Seacr output, creating .bed files containing peaks of minimum 'total signal' of threshold of 5, 8 and 10. Taking advantage of the five technical replicates one can also access the reproducibility of a called region. For each threshold, the overlap across the five technical replicates is calculated with intervene tools (Venn upset and pairwise) and a series of .bed files containing at least one (union of all technical replicates) to five (common among all technical replicates) are created using multiIntersectBed with -wa wb flags of bedtools version 2.30.0. Intersection between biological replicates can follow the same pipeline. This classification of peaks allows their quantification and ranking according to the normalized (cpm) signal strength as well as the reproducibility of the peak, allowing weaker but highly reproducible regions to be identified. All correlation analysis among a biological experiment was done on the consensus peaks, and correlation analysis between biological experiments and between different molecules on the union of the corresponding consensus sets, using deepTools[41]. Differential binding analysis follows DiffBind version 3.15 in R package pipeline version 4.2.2, using the deduplicated BAM files and consensus peaks, to create PCA, MA plots as well as calculate FRiP[42,43]. High-confidence peak regions, unless otherwise stated, are considered those regions at the top 1% by AUC, with minimum total signal 5 (min5) and present in three of five replicates (multi3). The highest-confidence *BRD4* binding sites in K562 cells were defined as peaks present across all technical and biological replicates in CUT&Tag (7,772 peaks).

Statistical analysis

Data are presented as mean ± s.d. The sample sizes (n) in the figure legends indicate the number of replicates in each experiment and are provided in the corresponding figure legends. The peak or gene size (N) in the heat maps indicates the number of peaks or genes included. Statistical analysis in Fig. 1 and Extended Data Figs. 2–3 was performed by unpaired Student's t tests, and the P values were denoted in each figure.

Reporting summary

Further information on research design is available in the Nature Portfolio Reporting Summary linked to this article.

Data availability

Sequencing data generated in this study have been submitted to the NCBI Gene Expression Omnibus (GEO; https://www.ncbi.nlm.nih.gov/geo/) under accession number GSE209713 (ref. [44]). The following previously published datasets were used: hg38 (https://www.ensembl.org/Homo_sapiens/Info/Index), JQ1 Click-Chem-seq (GSE88751)[5], ATAC-seq (GSE162299)[29], BG4 CUT&Tag (GSE181373)[24] and OQs (GSE110582)[23].

Code availability

All bioinformatics scripts are available on https://github.com/sblab-bioinformatics/Chem-map ref. [45].

References

40. Buenrostro, J. D. et al. Single-cell chromatin accessibility reveals principles of regulatory variation. *Nature* **523**, 486–490 (2015).
41. Ramírez, F. et al. deepTools2: a next generation web server for deep-sequencing data analysis. *Nucleic Acids Res.* **44**, W160–W165 (2016).
42. Ross-Innes, C. S. et al. Differential oestrogen receptor binding is associated with clinical outcome in breast cancer. *Nature* **481**, 389–393 (2012).
43. Stark, R. & Brown, G. DiffBind: differential binding analysis of ChIP-Seq peak data. http://bioconductor.org/packages/release/bioc/vignettes/DiffBind/inst/doc/DiffBind.pdf (2011).
44. Yu, Z. et al. Chem-map profiles drug binding to chromatin in cells. https://www.ncbi.nlm.nih.gov/geo/query/acc.cgi?acc=GSE209713 (2022).
45. Yu, Z. et al. Chem-map profiles drug binding to chromatin in cells. https://github.com/sblab-bioinformatics/Chem-map (2022).

Acknowledgements
We thank D. Tannahill from Cambridge University, UK and S. Aparicio from British Columbia Cancer Research Centre, Canada for their helpful discussion and comments on the manuscript. We thank the staff at the Genomic Core Facility at the Cancer Research UK Cambridge Institute for assistance with sequencing experiments. We thank P. Gierth (NMR Facility) for assistance in the NMR analysis. This work was financially supported by program grant funding from Cancer Research UK (C9681/A29214), core funding from Cancer Research UK (C9545/A19836) and Herchel Smith funds. S.B. is a Wellcome Trust Senior Investigator (209441/Z/17/Z).

Author contributions
Z.Y. and S.B. initiated the project. Z.Y., J.S. and S.B. conceived and designed the experiments. Z.Y. and J.S. performed the Chem-map experiments. L.M. performed the computational analysis of sequencing data and J.S. supported computational analysis. Z.Y. carried out experiments on chemical synthesis and biophysical evaluation. W.W.I.H. generated adapter-loaded pA–Tn5 and advised on CUT&Tag experiments. X.Z. and A.R. provided chemical intermediates for PDS and PhenDC3 synthesis. Z.Y., J.S., L.M. and S.B. interpreted the results. J.S. and Z.Y. generated the figures. Z.Y., J.S. and S.B. wrote the manuscript, with contributions from all the authors.

Competing interests
S.B. is a founder and shareholder of Cambridge Epigenetix and Inflex. J.S. is an employee of Inflex. The other authors declare no conflicts of interests.

Additional information
Extended data is available for this paper at https://doi.org/10.1038/s41587-022-01636-0.

Supplementary information The online version contains supplementary material available at https://doi.org/10.1038/s41587-022-01636-0.

Correspondence and requests for materials should be addressed to Shankar Balasubramanian.

Peer review information *Nature Biotechnology* thanks Raphaël Rodriguez and the other, anonymous, reviewer(s) for their contribution to the peer review of this work.

https://doi.org/10.1038/s41587-022-01636-0

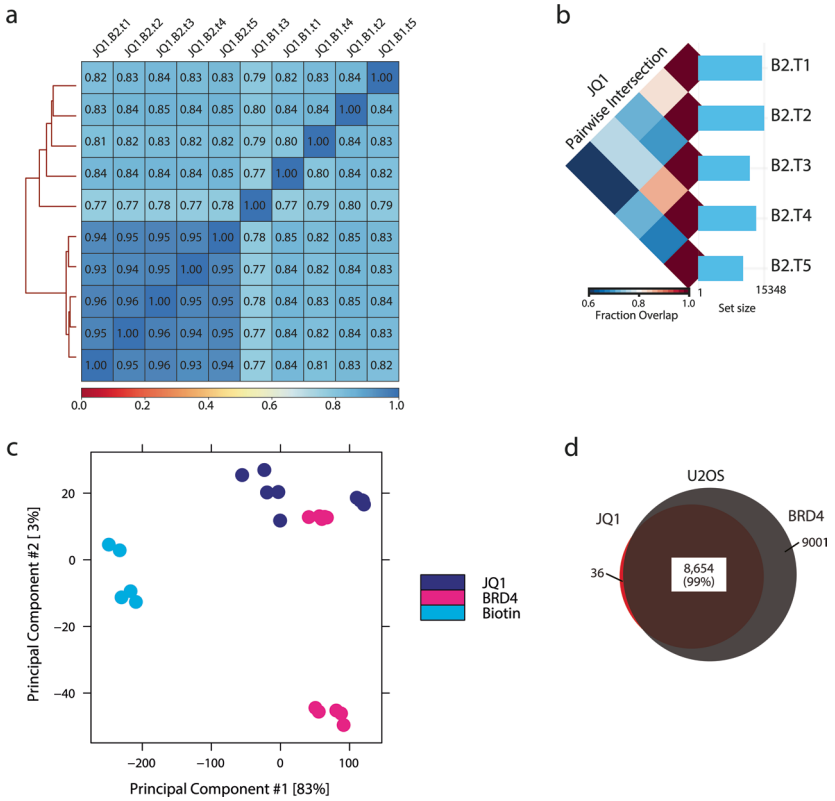

Extended Data Fig. 1 | Characterization of Chem-map for JQ1. (**a**) Hierarchical clustering of the Spearman correlation matrix for two biological replicates of JQ1 Chem-map in K562 cells each with 5 technical replicates. (**b**) Pairwise intersection of enriched peaks from JQ1 Chem-map in K562 cells for a 2nd biological replicate comprising five technical replicates. (**c**) Principal components analysis (PCA) comparing JQ1 Chem-map, biotin Chem-map, and BRD4 CUT&Tag in K562 cells. (**d**) Venn diagram illustrating the high-confidence binding sites of JQ1 (Chem-map, red) and its protein target BRD4 (CUT&Tag, black) in U2OS cells.

https://doi.org/10.1038/s41587-022-01636-0

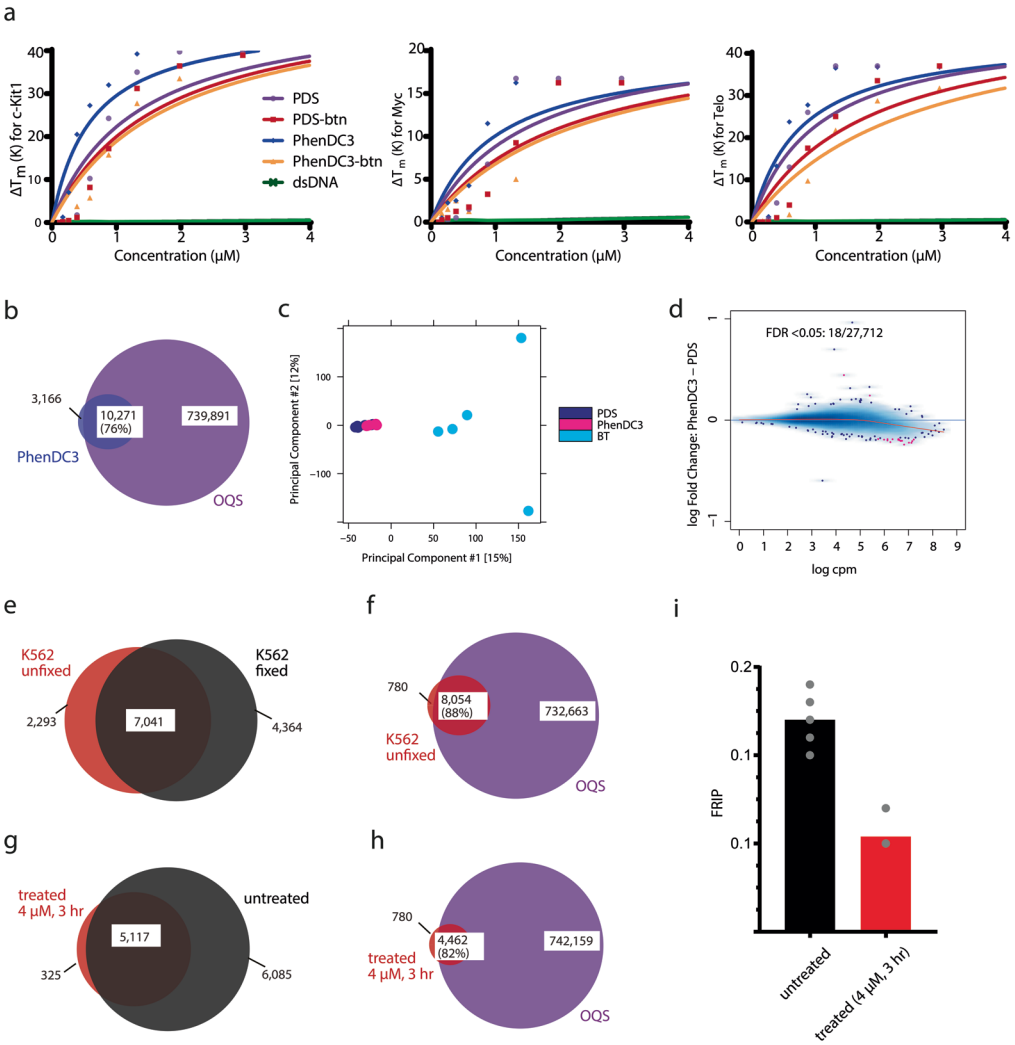

Extended Data Fig. 2 | Chem-map data for G4 ligands (PDS and PhenDC). **(a)** FRET-melting assay of G4 ligand binding to G4-forming oligonucleotides (c-Kit, Myc, and Telo) and negative control dsDNA with inducing thermal stabilization (ΔT_m). Mean is represented from two independent experiments ($n = 2$). **(b)** Venn diagrams illustrating the overlap of binding sites for the G4 ligands PhenDC3 and OQS. **(c)** Differential binding analysis for PDS Chem-map and PhenDC3 Chem-map. **(d)** Principal components analysis (PCA) comparing Chem-map experiments with G4 ligands and biotin control in K562 cells. **(e)** Venn diagrams illustrating the overlap of PDS Chem-map high-confidence peaks from lightly fixed and unfixed K562 cells (present in 3/5 technical replicates) and the respective overlap with OQS (**f**). (**g**) Venn diagrams illustrating the overlap of PDS Chem-map high-confidence peaks from K562 cells (present in 3/5 technical replicates) dosed with unmodified PDS (4 μM for 3 h) and overlap of those peaks with OQS (**h**). (**i**) FRiP analysis comparing untreated and treated (unmodified PDS, 4 μM for 3 h) PDS Chem-map in K562 cells ($n = 5$).

https://doi.org/10.1038/s41587-022-01636-0

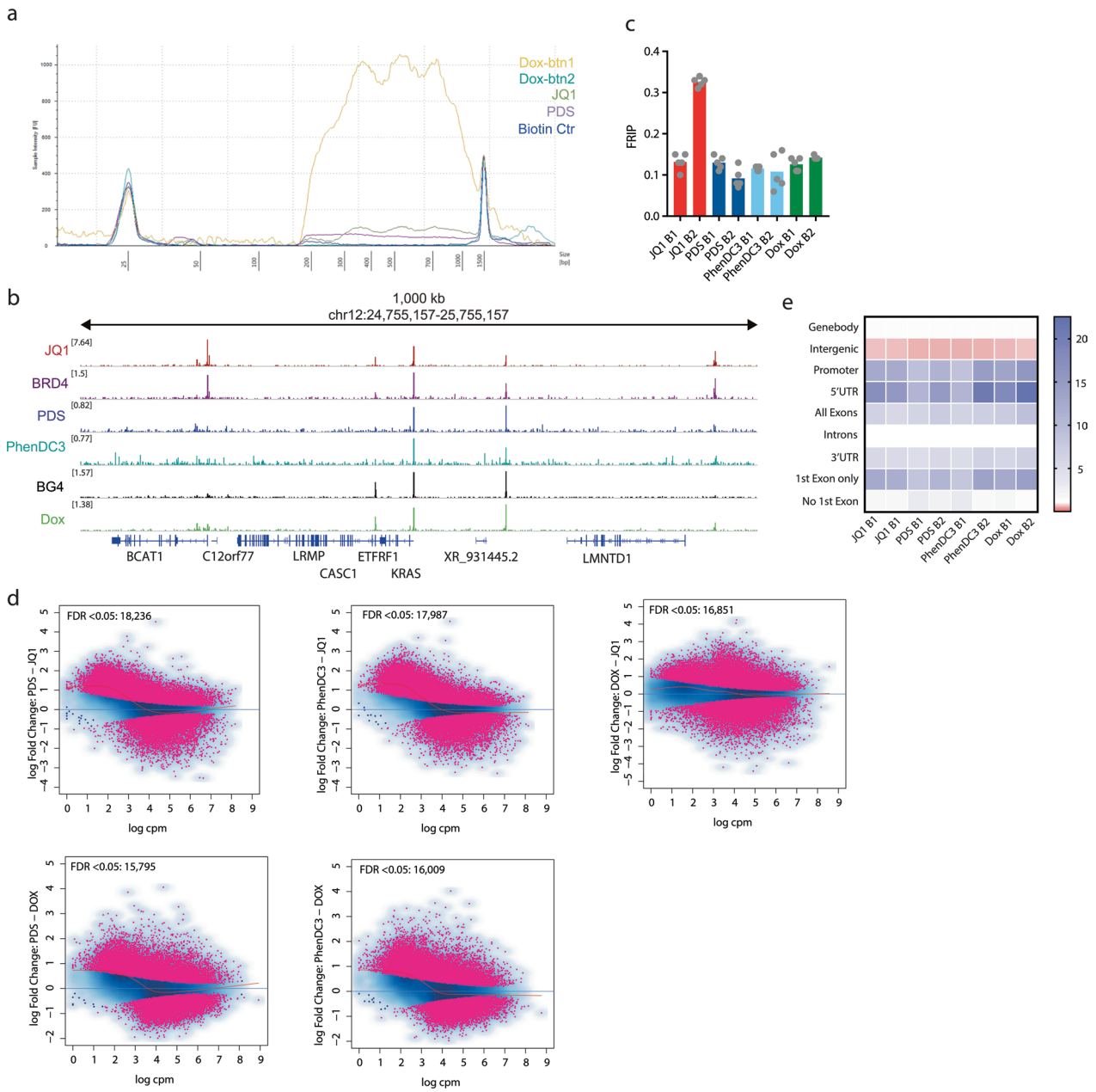

Extended Data Fig. 3 | Characterization of Chem-map datasets with different small molecules. (**a**) Tapestation analysis comparing relative DNA recovery after PCR for Dox-btn1, Dox-btn2, JQ1-btn, PDS-btn, PhenDC3-btn, and biotin control. (**b**) Gene browser views of peak profiles among JQ1 Chem-map, BRD4 CUT&Tag, PDS Chem-map, PhenDC3 Chem-map, BG4 CUT&Tag, and doxorubicin Chem-map. (**c**) FRiP analysis of Chem-map with different small molecules in K562 cells. (**d**) Differential binding analysis (FDR < 0.05) for Chem-map comparing binding sites for different small molecules in K562 cells. Red dots represent sites where the binding is significantly different for two molecules (considering two biological replicates each with five technical replicates). (**e**) Enrichment over random (n = 1,000 permutations) of JQ1, PDS, PhenDC3 and Doxorubicin at genomic features from the reference human annotation GENECODE v.28. UTR untranslated region; Promoter defined as 1 kb upstream transcription start sites. Peak distribution of Chem-map experiment with JQ1, PDS, PhenDC3, and doxorubicin, across different genomic features.

https://doi.org/10.1038/s41587-022-01636-0

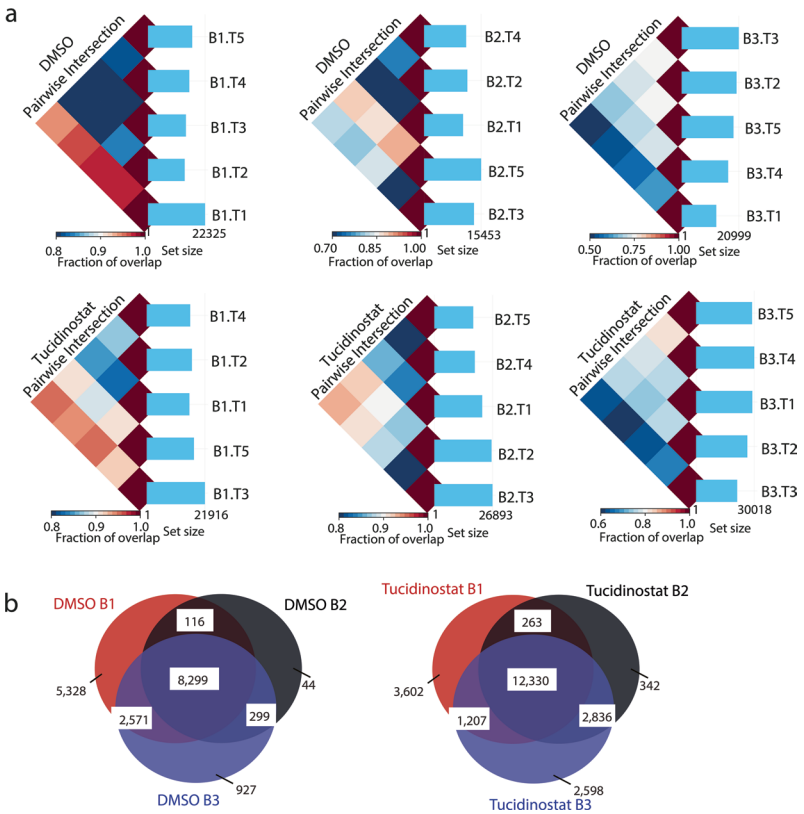

Extended Data Fig. 4 | Characterization of Dox-btn1 Chem-map for tucidinostat. (**a**) Pairwise intersection of enriched peaks from Dox-btn1 Chem-map for DMSO vehicle control- and tucidinostat-treated K562 cells. (**b**) Venn diagram comparing high-confidence binding sites for three biological replicates of Dox-btn1 Chem-map in vehicle control- and tucidinostat-treated K562 cells.

nature portfolio

Corresponding author(s): Shankar Balasubramanian

Last updated by author(s): Oct 28, 2022

Reporting Summary

Nature Portfolio wishes to improve the reproducibility of the work that we publish. This form provides structure for consistency and transparency in reporting. For further information on Nature Portfolio policies, see our Editorial Policies and the Editorial Policy Checklist.

Statistics

For all statistical analyses, confirm that the following items are present in the figure legend, table legend, main text, or Methods section.

n/a	Confirmed
☐	☒ The exact sample size (*n*) for each experimental group/condition, given as a discrete number and unit of measurement
☐	☒ A statement on whether measurements were taken from distinct samples or whether the same sample was measured repeatedly
☐	☒ The statistical test(s) used AND whether they are one- or two-sided *Only common tests should be described solely by name; describe more complex techniques in the Methods section.*
☒	☐ A description of all covariates tested
☒	☐ A description of any assumptions or corrections, such as tests of normality and adjustment for multiple comparisons
☐	☒ A full description of the statistical parameters including central tendency (e.g. means) or other basic estimates (e.g. regression coefficient) AND variation (e.g. standard deviation) or associated estimates of uncertainty (e.g. confidence intervals)
☐	☒ For null hypothesis testing, the test statistic (e.g. *F*, *t*, *r*) with confidence intervals, effect sizes, degrees of freedom and *P* value noted *Give P values as exact values whenever suitable.*
☒	☐ For Bayesian analysis, information on the choice of priors and Markov chain Monte Carlo settings
☒	☐ For hierarchical and complex designs, identification of the appropriate level for tests and full reporting of outcomes
☒	☐ Estimates of effect sizes (e.g. Cohen's *d*, Pearson's *r*), indicating how they were calculated

Our web collection on statistics for biologists contains articles on many of the points above.

Software and code

Policy information about availability of computer code

Data collection	Bruker 400 MHz Avance III HD Spectrometer, 500 MHz DCH Cryoprobe Spectrometer, Waters Vion IMS QTof spectrometer, Bio-Rad CFX96 Touch Real-Time PCR Detection System, Agilent TapeStation, EVOS M5000 449 microscope (Thermo Fisher Scientific), and NextSeq 500 sequencer (Illumina)
Data analysis	Agilent TapeStation, NMR data was processed in MestReNova (version 14.2.3), Binding data for FRET melting assay were processed with Prism 8 (GraphPad Software Inc.). Bioinformatics data analyses and processing were performed using Bash and R (v 4.2.2) programming languages. The following tools were also used: demuxIllumina (v 3.0.9), fastQC (v0.11.8), MultiQC v1.11, cutadapt (v 1.16), BWA (0.7.17-r1188), Picard (v 2.20.3), Seacr (v1.3), bedtools57 (v.2.30.0), deepTools (v 2.0), DiffBind (v3.15). Scripts genomics analyses available in the github page dedicated to this study: https://github.com/sblab-bioinformatics/Chem-map

For manuscripts utilizing custom algorithms or software that are central to the research but not yet described in published literature, software must be made available to editors and reviewers. We strongly encourage code deposition in a community repository (e.g. GitHub). See the Nature Portfolio guidelines for submitting code & software for further information.

Data

Policy information about availability of data

All manuscripts must include a data availability statement. This statement should provide the following information, where applicable:

- Accession codes, unique identifiers, or web links for publicly available datasets
- A description of any restrictions on data availability
- For clinical datasets or third party data, please ensure that the statement adheres to our policy

Sequencing data generated in this study have been submitted to the NCBI Gene Expression Omnibus (GEO; https://www.ncbi.nlm.nih.gov/geo/) under accession number GSE209713. The following previously published datasets were used: hg38, JQ1 Click-Chem-seq (GSE88751), ATAC-seq (GSE162299), BG4 CUT&Tag (GSE181373), and OQs (GSE110582).

Human research participants

Policy information about studies involving human research participants and Sex and Gender in Research.

Reporting on sex and gender	n/a
Population characteristics	n/a
Recruitment	n/a
Ethics oversight	n/a

Note that full information on the approval of the study protocol must also be provided in the manuscript.

Field-specific reporting

Please select the one below that is the best fit for your research. If you are not sure, read the appropriate sections before making your selection.

☒ Life sciences ☐ Behavioural & social sciences ☐ Ecological, evolutionary & environmental sciences

For a reference copy of the document with all sections, see nature.com/documents/nr-reporting-summary-flat.pdf

Life sciences study design

All studies must disclose on these points even when the disclosure is negative.

Sample size	1 x 105 U2OS cells were seeded in 12-well plate to ensure 70-80% cell confluence for imaging study. According to previous study of CUT&Tag (Kaya-Okur, H.S. et al. Nat. Commun. 10, 1930 (2019)), cell numbers ranging from 1 x 105 to 5 x 105 cells and 10 uL conA beads were applied. In this study, Brd4 CUT&Tag study used 1 x 105 cells and 10 uL conA beads per sample. For Chem-map, considering binding affinity difference, we increased to 6 x 105 cells and 15 uL conA beads.
Data exclusions	No data were excluded from analyses.
Replication	Chem-map and CUT&Tag experiments were performed in at least 2 biological replicates comprising 5 technical replicates to ensure reproducibility. FRET melting experiments were performed in three technical replicates for each oligomer and mean is represented from two independent experiments (n=2). All experiments provided consistent and reproducible measurements.
Randomization	After U2OS cells were seeded in slides, we randomly decided the treatment wells.
Blinding	No animals or human participants were used in studies. It is not applied to molecule and cellular experiments.

Behavioural & social sciences study design

All studies must disclose on these points even when the disclosure is negative.

Study description	*Briefly describe the study type including whether data are quantitative, qualitative, or mixed-methods (e.g. qualitative cross-sectional, quantitative experimental, mixed-methods case study).*

Research sample	*State the research sample (e.g. Harvard university undergraduates, villagers in rural India) and provide relevant demographic information (e.g. age, sex) and indicate whether the sample is representative. Provide a rationale for the study sample chosen. For studies involving existing datasets, please describe the dataset and source.*
Sampling strategy	*Describe the sampling procedure (e.g. random, snowball, stratified, convenience). Describe the statistical methods that were used to predetermine sample size OR if no sample-size calculation was performed, describe how sample sizes were chosen and provide a rationale for why these sample sizes are sufficient. For qualitative data, please indicate whether data saturation was considered, and what criteria were used to decide that no further sampling was needed.*
Data collection	*Provide details about the data collection procedure, including the instruments or devices used to record the data (e.g. pen and paper, computer, eye tracker, video or audio equipment) whether anyone was present besides the participant(s) and the researcher, and whether the researcher was blind to experimental condition and/or the study hypothesis during data collection.*
Timing	*Indicate the start and stop dates of data collection. If there is a gap between collection periods, state the dates for each sample cohort.*
Data exclusions	*If no data were excluded from the analyses, state so OR if data were excluded, provide the exact number of exclusions and the rationale behind them, indicating whether exclusion criteria were pre-established.*
Non-participation	*State how many participants dropped out/declined participation and the reason(s) given OR provide response rate OR state that no participants dropped out/declined participation.*
Randomization	*If participants were not allocated into experimental groups, state so OR describe how participants were allocated to groups, and if allocation was not random, describe how covariates were controlled.*

Ecological, evolutionary & environmental sciences study design

All studies must disclose on these points even when the disclosure is negative.

Study description	*Briefly describe the study. For quantitative data include treatment factors and interactions, design structure (e.g. factorial, nested, hierarchical), nature and number of experimental units and replicates.*
Research sample	*Describe the research sample (e.g. a group of tagged Passer domesticus, all Stenocereus thurberi within Organ Pipe Cactus National Monument), and provide a rationale for the sample choice. When relevant, describe the organism taxa, source, sex, age range and any manipulations. State what population the sample is meant to represent when applicable. For studies involving existing datasets, describe the data and its source.*
Sampling strategy	*Note the sampling procedure. Describe the statistical methods that were used to predetermine sample size OR if no sample-size calculation was performed, describe how sample sizes were chosen and provide a rationale for why these sample sizes are sufficient.*
Data collection	*Describe the data collection procedure, including who recorded the data and how.*
Timing and spatial scale	*Indicate the start and stop dates of data collection, noting the frequency and periodicity of sampling and providing a rationale for these choices. If there is a gap between collection periods, state the dates for each sample cohort. Specify the spatial scale from which the data are taken*
Data exclusions	*If no data were excluded from the analyses, state so OR if data were excluded, describe the exclusions and the rationale behind them, indicating whether exclusion criteria were pre-established.*
Reproducibility	*Describe the measures taken to verify the reproducibility of experimental findings. For each experiment, note whether any attempts to repeat the experiment failed OR state that all attempts to repeat the experiment were successful.*
Randomization	*Describe how samples/organisms/participants were allocated into groups. If allocation was not random, describe how covariates were controlled. If this is not relevant to your study, explain why.*
Blinding	*Describe the extent of blinding used during data acquisition and analysis. If blinding was not possible, describe why OR explain why blinding was not relevant to your study.*

Did the study involve field work? ☐ Yes ☐ No

Field work, collection and transport

Field conditions	*Describe the study conditions for field work, providing relevant parameters (e.g. temperature, rainfall).*
Location	*State the location of the sampling or experiment, providing relevant parameters (e.g. latitude and longitude, elevation, water depth).*
Access & import/export	*Describe the efforts you have made to access habitats and to collect and import/export your samples in a responsible manner and in*

Access & import/export	*compliance with local, national and international laws, noting any permits that were obtained (give the name of the issuing authority, the date of issue, and any identifying information).*
Disturbance	*Describe any disturbance caused by the study and how it was minimized.*

Reporting for specific materials, systems and methods

We require information from authors about some types of materials, experimental systems and methods used in many studies. Here, indicate whether each material, system or method listed is relevant to your study. If you are not sure if a list item applies to your research, read the appropriate section before selecting a response.

Materials & experimental systems

n/a	Involved in the study
☐	☒ Antibodies
☐	☒ Eukaryotic cell lines
☒	☐ Palaeontology and archaeology
☒	☐ Animals and other organisms
☒	☐ Clinical data
☒	☐ Dual use research of concern

Methods

n/a	Involved in the study
☒	☐ ChIP-seq
☒	☐ Flow cytometry
☒	☐ MRI-based neuroimaging

Antibodies

Antibodies used	concanavalin A-coated magnetic beads (Bangs Labs, BP531), anti-biotin (D5A7) Rabbit mAb (Cell Signaling Technology, 5597), anti-BRD4 (E2A7X) antibody (Cell Signalling Technology, 13440), Guinea Pig anti-rabbit antibody (Antibodies-Online, ABIN101961)
Validation	Commercial antibodies and beads had been validated by the manufacturers: concanavalin A-coated magnetic beads has been used in previous studies (Kaya-Okur, H.S. et al. Nat. Commun. 10, 1930 (2019)) and see also: https://www.bangslabs.com/products/magnetic-microspheres-particles/biomag-biomag-plus-binding-proteins anti-biotin (D5A7) Rabbit mAb has been tested in WB, CUT&Tag, CUT&RUN, ChIP, IP and IF: https://www.cellsignal.com/products/secondary-antibodies/anti-biotin-d5a7-rabbit-mab/5597 anti-BRD4 (E2A7X) antibody has been tested in WB, CUT&Tag, CUT&RUN, ChIP, IP and IF: https://www.cellsignal.com/products/primary-antibodies/brd4-e2a7x-rabbit-mab/13440 Guinea Pig anti-rabbit antibody has been tested in WB, CUT&Tag, CUT&RUN, ELISA and IHC: https://www.antibodies-online.com/antibody/101961/Guinea+Pig+anti-Rabbit+IgG+Heavy++Light+Chain+antibody+-+Preadsorbed/

Eukaryotic cell lines

Policy information about cell lines and Sex and Gender in Research

Cell line source(s)	human chronic myelogenous leukemia K562 cells (RRID:CVCL 0004) were purchased from ATCC human bone osteosarcoma epithelial U2OS cells (RRID:CVCL_0042) were obtained from ATCC
Authentication	Short tandem repeat (STR) profiling was used to distinguish between individual human cell lines and rule out intra-species contamination performed by the CRUK Cambridge Institute Biorepository Core Facility.
Mycoplasma contamination	Cells were tested mycoplasma-free based on RNA-capture ELISA performed by the CRUK Cambridge Institute Biorepository Core Facility.
Commonly misidentified lines (See ICLAC register)	No commonly misidentified cell lines were used.

Palaeontology and Archaeology

Specimen provenance	*Provide provenance information for specimens and describe permits that were obtained for the work (including the name of the issuing authority, the date of issue, and any identifying information). Permits should encompass collection and, where applicable, export.*
Specimen deposition	*Indicate where the specimens have been deposited to permit free access by other researchers.*
Dating methods	*If new dates are provided, describe how they were obtained (e.g. collection, storage, sample pretreatment and measurement), where they were obtained (i.e. lab name), the calibration program and the protocol for quality assurance OR state that no new dates are provided.*

☐ Tick this box to confirm that the raw and calibrated dates are available in the paper or in Supplementary Information.

Ethics oversight	*Identify the organization(s) that approved or provided guidance on the study protocol, OR state that no ethical approval or guidance was required and explain why not.*

Note that full information on the approval of the study protocol must also be provided in the manuscript.

Animals and other research organisms

Policy information about studies involving animals; ARRIVE guidelines recommended for reporting animal research, and Sex and Gender in Research

Laboratory animals	*For laboratory animals, report species, strain and age OR state that the study did not involve laboratory animals.*
Wild animals	*Provide details on animals observed in or captured in the field; report species and age where possible. Describe how animals were caught and transported and what happened to captive animals after the study (if killed, explain why and describe method; if released, say where and when) OR state that the study did not involve wild animals.*
Reporting on sex	*Indicate if findings apply to only one sex; describe whether sex was considered in study design, methods used for assigning sex. Provide data disaggregated for sex where this information has been collected in the source data as appropriate; provide overall numbers in this Reporting Summary. Please state if this information has not been collected. Report sex-based analyses where performed, justify reasons for lack of sex-based analysis.*
Field-collected samples	*For laboratory work with field-collected samples, describe all relevant parameters such as housing, maintenance, temperature, photoperiod and end-of-experiment protocol OR state that the study did not involve samples collected from the field.*
Ethics oversight	*Identify the organization(s) that approved or provided guidance on the study protocol, OR state that no ethical approval or guidance was required and explain why not.*

Note that full information on the approval of the study protocol must also be provided in the manuscript.

Clinical data

Policy information about clinical studies

All manuscripts should comply with the ICMJE guidelines for publication of clinical research and a completed CONSORT checklist must be included with all submissions.

Clinical trial registration	*Provide the trial registration number from ClinicalTrials.gov or an equivalent agency.*
Study protocol	*Note where the full trial protocol can be accessed OR if not available, explain why.*
Data collection	*Describe the settings and locales of data collection, noting the time periods of recruitment and data collection.*
Outcomes	*Describe how you pre-defined primary and secondary outcome measures and how you assessed these measures.*

Dual use research of concern

Policy information about dual use research of concern

Hazards

Could the accidental, deliberate or reckless misuse of agents or technologies generated in the work, or the application of information presented in the manuscript, pose a threat to:

No	Yes	
☐	☐	Public health
☐	☐	National security
☐	☐	Crops and/or livestock
☐	☐	Ecosystems
☐	☐	Any other significant area

Experiments of concern

Does the work involve any of these experiments of concern:

No	Yes	
☐	☐	Demonstrate how to render a vaccine ineffective
☐	☐	Confer resistance to therapeutically useful antibiotics or antiviral agents
☐	☐	Enhance the virulence of a pathogen or render a nonpathogen virulent
☐	☐	Increase transmissibility of a pathogen
☐	☐	Alter the host range of a pathogen
☐	☐	Enable evasion of diagnostic/detection modalities
☐	☐	Enable the weaponization of a biological agent or toxin
☐	☐	Any other potentially harmful combination of experiments and agents

ChIP-seq

Data deposition

☐ Confirm that both raw and final processed data have been deposited in a public database such as GEO.

☐ Confirm that you have deposited or provided access to graph files (e.g. BED files) for the called peaks.

Data access links *May remain private before publication.*	*For "Initial submission" or "Revised version" documents, provide reviewer access links. For your "Final submission" document, provide a link to the deposited data.*
Files in database submission	*Provide a list of all files available in the database submission.*
Genome browser session (e.g. UCSC)	*Provide a link to an anonymized genome browser session for "Initial submission" and "Revised version" documents only, to enable peer review. Write "no longer applicable" for "Final submission" documents.*

Methodology

Replicates	*Describe the experimental replicates, specifying number, type and replicate agreement.*
Sequencing depth	*Describe the sequencing depth for each experiment, providing the total number of reads, uniquely mapped reads, length of reads and whether they were paired- or single-end.*
Antibodies	*Describe the antibodies used for the ChIP-seq experiments; as applicable, provide supplier name, catalog number, clone name, and lot number.*
Peak calling parameters	*Specify the command line program and parameters used for read mapping and peak calling, including the ChIP, control and index files used.*
Data quality	*Describe the methods used to ensure data quality in full detail, including how many peaks are at FDR 5% and above 5-fold enrichment.*
Software	*Describe the software used to collect and analyze the ChIP-seq data. For custom code that has been deposited into a community repository, provide accession details.*

Flow Cytometry

Plots

Confirm that:

☐ The axis labels state the marker and fluorochrome used (e.g. CD4-FITC).

☐ The axis scales are clearly visible. Include numbers along axes only for bottom left plot of group (a 'group' is an analysis of identical markers).

☐ All plots are contour plots with outliers or pseudocolor plots.

☐ A numerical value for number of cells or percentage (with statistics) is provided.

Methodology

Sample preparation	*Describe the sample preparation, detailing the biological source of the cells and any tissue processing steps used.*
Instrument	*Identify the instrument used for data collection, specifying make and model number.*

Software

Describe the software used to collect and analyze the flow cytometry data. For custom code that has been deposited into a community repository, provide accession details.

Cell population abundance

Describe the abundance of the relevant cell populations within post-sort fractions, providing details on the purity of the samples and how it was determined.

Gating strategy

Describe the gating strategy used for all relevant experiments, specifying the preliminary FSC/SSC gates of the starting cell population, indicating where boundaries between "positive" and "negative" staining cell populations are defined.

☐ Tick this box to confirm that a figure exemplifying the gating strategy is provided in the Supplementary Information.

Magnetic resonance imaging

Experimental design

Design type

Indicate task or resting state; event-related or block design.

Design specifications

Specify the number of blocks, trials or experimental units per session and/or subject, and specify the length of each trial or block (if trials are blocked) and interval between trials.

Behavioral performance measures

State number and/or type of variables recorded (e.g. correct button press, response time) and what statistics were used to establish that the subjects were performing the task as expected (e.g. mean, range, and/or standard deviation across subjects).

Acquisition

Imaging type(s)

Specify: functional, structural, diffusion, perfusion.

Field strength

Specify in Tesla

Sequence & imaging parameters

Specify the pulse sequence type (gradient echo, spin echo, etc.), imaging type (EPI, spiral, etc.), field of view, matrix size, slice thickness, orientation and TE/TR/flip angle.

Area of acquisition

State whether a whole brain scan was used OR define the area of acquisition, describing how the region was determined.

Diffusion MRI ☐ Used ☐ Not used

Preprocessing

Preprocessing software

Provide detail on software version and revision number and on specific parameters (model/functions, brain extraction, segmentation, smoothing kernel size, etc.).

Normalization

If data were normalized/standardized, describe the approach(es): specify linear or non-linear and define image types used for transformation OR indicate that data were not normalized and explain rationale for lack of normalization.

Normalization template

Describe the template used for normalization/transformation, specifying subject space or group standardized space (e.g. original Talairach, MNI305, ICBM152) OR indicate that the data were not normalized.

Noise and artifact removal

Describe your procedure(s) for artifact and structured noise removal, specifying motion parameters, tissue signals and physiological signals (heart rate, respiration).

Volume censoring

Define your software and/or method and criteria for volume censoring, and state the extent of such censoring.

Statistical modeling & inference

Model type and settings

Specify type (mass univariate, multivariate, RSA, predictive, etc.) and describe essential details of the model at the first and second levels (e.g. fixed, random or mixed effects; drift or auto-correlation).

Effect(s) tested

Define precise effect in terms of the task or stimulus conditions instead of psychological concepts and indicate whether ANOVA or factorial designs were used.

Specify type of analysis: ☐ Whole brain ☐ ROI-based ☐ Both

Statistic type for inference
(See Eklund et al. 2016)

Specify voxel-wise or cluster-wise and report all relevant parameters for cluster-wise methods.

Correction

Describe the type of correction and how it is obtained for multiple comparisons (e.g. FWE, FDR, permutation or Monte Carlo).

Models & analysis

n/a	Involved in the study
☐	☐ Functional and/or effective connectivity
☐	☐ Graph analysis
☐	☐ Multivariate modeling or predictive analysis

Functional and/or effective connectivity

Report the measures of dependence used and the model details (e.g. Pearson correlation, partial correlation, mutual information).

Graph analysis

Report the dependent variable and connectivity measure, specifying weighted graph or binarized graph, subject- or group-level, and the global and/or node summaries used (e.g. clustering coefficient, efficiency, etc.).

Multivariate modeling and predictive analysis

Specify independent variables, features extraction and dimension reduction, model, training and evaluation metrics.